Materials Research
Express

PAPER • **OPEN ACCESS**

Simulation of salt spray corrosion behaviour of micro-arc oxidation coating by laser induced Ag infiltration

To cite this article: Cancan Liu *et al* 2020 *Mater. Res. Express* **7** 016434

Materials Research Express

OPEN ACCESS

RECEIVED
12 November 2019

REVISED
2 January 2020

ACCEPTED FOR PUBLICATION
13 January 2020

PUBLISHED
27 January 2020

PAPER

Simulation of salt spray corrosion behaviour of micro-arc oxidation coating by laser induced Ag infiltration

Cancan Liu[1], **Hongtao Li**[1,2], **Hailong Cai**[1], **L A Angurel**[2], **G F de la Fuente**[2] **and Bailing Jiang**[1]

[1] College of Materials Science and Engineering, Nanjing Tech University, Nanjing, 211816, People's Republic of China
[2] Instituto de Ciencia de Materiales de Aragón (CSIC-Universidad de Zaragoza), Zaragoza, 50018, Spain

E-mail: lihongtao@njtech.edu.cn

Keywords: simulation, micro-arc oxidation, corrosion channels, Ag tracer, laser irradiation

Abstract

Micro-arc oxidation (MAO) coating was initially prepared on 6061 Al alloy, and subsequently coated with Ag using magnetron sputtering. Laser beam scan (LBS) treatments were then applied to infiltrate the sputtered Ag into the MAO coating in order to simulate the corrosion behaviour of the MAO coating during the neutral salt spray test (NSST). Cross-sectional morphologies and Ag element distribution maps were studied by using the field emission scanning electron microscopy (FESEM) on the MAO-Ag coated samples after LBS infiltration. The results showed that there existed the micro-cracks with tree-root or lightning shape within the MAO coating. Interconnected aggregates, including micro-pores, large cavities far beneath the surface and tree-root like micro-cracks, served as complex corrosion channels during salt spray corrosion. Through these corrosion channels, the salt spray penetrated gradually into the interface between the MAO coating and the original Al substrate, thus causing corrosion of the Al substrate during the NSST. The LBS treatment is presented as a method to explore the subtle micro-crack and pore channels associated to the MAO coating and to provide information that paves the way towards understanding of corrosion phenomena in these porous systems.

1. Introduction

Micro-arc oxidation (MAO) is an effective surface treatment technique to fabricate the metallurgical oxide coatings on the surface of aluminum (Al) and its alloys, utilizing a micro-arc discharge generated by dielectric breakdown [1–3]. Owing to the high temperatures generated during the micro-arc discharge, Al atoms within the substrate micro-zone react with the oxygen plasma [4–6]. A thick and hard ceramic oxide coating is prepared on Al alloys. Hence, MAO treatment can effectively improve the mechanical and corrosion properties of Al alloys for applications in various industrial branches, such as aerospace, automotive, naval, biomedicine, electronics and energy [7–11].

Various methods are applied to evaluate the corrosion resistance of MAO coatings on Al alloys, such as electrochemical corrosion, immersion or salt spray tests [12–14]. Among these methods, the neutral salt spray test (NSST) is one of the most common and simple means to assess the corrosion performance [14–16]. However, much attention was paid to the consequences of the salt spray test, whereas relatively neglected to trace the corrosion sequential process and observe corrosion channels induced during the salt spray test [14–16]. These were owing to the fact that most corrosion channels were locally destroyed due to the formation of corrosion products during the NSST. In addition, it was difficult to observe directly the distribution of corrosion products within the cross-sectional direction after the NSST. Tracing the corrosion sequential process and observing corrosion channels are critical to understand the corrosion mechanism of the MAO coated Al alloys, in order to improve the corrosion resistance of MAO coatings.

In this work, silver (Ag), a stable chemical element with strong mechanical adhesion and high thermal conductivity, was employed as the accessible tracer [17, 18]. Al_2O_3 was proved to be the main constituent for the

MAO coatings on Al alloys [19, 20]. In view of the large differences in melting temperature and thermal expansion coefficient between Ag and Al_2O_3, laser irradiation in laser beam scan (LBS) mode was applied to infiltrate Ag into the porous MAO coating [21]. The salt spray infiltration process into the MAO coating during the NSST was simulated by the diffusion behaviour of Ag into an equivalent MAO coating. Besides, corrosion channels during the NSST were reflected by tracking of Ag infiltration paths. In this manner, the salt spray corrosion sequence, corrosion channels through the coatings and their fine microstructures can be illustrated in a straightforward way. The outcome of this work has important reference significance for the analysis of the corrosion behaviour of the MAO treated light alloys in the industry, especially the study of corrosion process before pitting.

2. Methods

2.1. Preparation of MAO coating

The substrate used in this study was 6061 Al alloy with the nominal composition (mass fraction): 0.15%–0.4% Cu, 0.8%–1.2% Mg, 0.15% Mn, 0.25% Zn, 0.04%–0.35% Cr, 0.15% Ti, 0.4%–0.8% Si, 0.7% Fe and balance Al, which was was supplied by Jiangsu Yimai aluminum industry Co., Ltd, China). Prior to surface treatment, the circular specimens with a diameter of 35 mm and a thickness of 3 mm were ground successively with SiC papers up to 1500 grit, degreased with acetone, washed with distilled water and dried in cool air stream.

A unipolar pulse power supply (Nanjing HaoRang Environment Science & Technology CO. Ltd, China) was used to prepare MAO coating. The MAO process was carried out in 20 g l^{-1} Na_2SiO_4, 3 g l^{-1} Na_2WO_4 and 5 g l^{-1} NaOH solution under constant current mode characterized using the following processing parameters: current density 4 A dm^{-2}, frequency 500 Hz, pulse width 80 μs and oxidation time 20 min. The solution temperature was kept below 30 °C with a stirring and water cooling system. During the MAO process, the voltage increased to breakdown voltage (247 V) about 30 s later. After the MAO treatment, samples were ultrasonically rinsed with distilled water for 10 min to eliminate the adsorbed solute anions.

2.2. Preparation of MAO-Ag composite coating

The Ag coating was deposited on the surface of MAO coating using a magnetron sputtering ion plating system (MSIP019). This system was equipped with one circular vertical magnetron (100 mm in diameter) installed in the chamber wall. The sputter Ag target (100 mm in diameter and 4 mm thick) is 99.9% pure (Shaanxi Sirui Industries Ltd, Xi'an, China). The substrate holder was designed to fix the substrate-to-target separation (d_{s-t}) at 120 mm with the rotation speed fixed at 8 rpm. Before deposition, the chamber was evacuated to a basic pressure lower than 3.0×10^{-5} Torr, and then backfilled with high purity argon (99.99%) to the required depositing pressure (about 8.4×10^{-4} Torr), as measured using a capacitance manometer gauge. During the deposition process, the Ag target current was 2 A and the deposition time was 30 min.

2.3. Laser induced silver infiltration process

Laser treatments to infiltrate the Ag into the MAO coating were performed using two different lasers in Laser Beam Scan (LBS) mode: an ns n-IR Yb fiber laser and a 300 ps UV laser. The laser beam scan process has been described elsewhere [22, 23]. The first laser treatment was performed using the following parameters: a maximum power of 20 W, wavelength of 1 μm, spot size of 36 μm and pulse duration from 4 ns to 200 ns. The objective of this laser treatment was to infiltrate the Ag into the MAO coating. In order to control the heat affected zone precisely and to reduce its thickness to a minimum, as well as to improve the Ag infiltration process, the UV laser (Rofin-sinar laser, Powerline Pico 10-355) was alternatively used. This laser emitted at 355 nm, with a maximum average power of 3 W, a pulse width of 300 ps and a beam diameter of 34 μm.

2.4. Characterization methods

The thickness of MAO coating was measured using an FMP20 eddy current thickness measurement gauge (Helmut Fischer GMBH, Sindelfingen, Germany) with an accuracy of 0.1 μm. Neutral salt spray test was conducted per GB/T 10125-2012/ISO 9227: 2006 standards to evaluate the long-term corrosion behaviour of the MAO treated Al alloy. Specimens were exposed to 5 wt% NaCl spray at 35 $\pm$ 2 °C for a duration of 1200 h. The 5 wt% NaCl solution was prepared using NaCl in distilled water with trace amounts of NaOH, and the pH value of this solution was 6.71 at 25 $\pm$ 2 °C. A digital camera was used to take photos of specimens after certain periods. After the salt spray test, the surface corrosion morphology of the MAO coating was observed by an Ultra55 field emission scanning electron microscopy (FESEM, Zeiss, Germany). The cross-sectional morphology and Ag element mappings of the MAO-Ag coating after laser infiltration were studied with FESEM (Carl Zeiss Merlin). The porosities of MAO and MAO/Ag coatings were approximately calculated using ImageJ software based on the surface FESEM micrographs. Tensile test was carried out using the WE-600 hydraulic

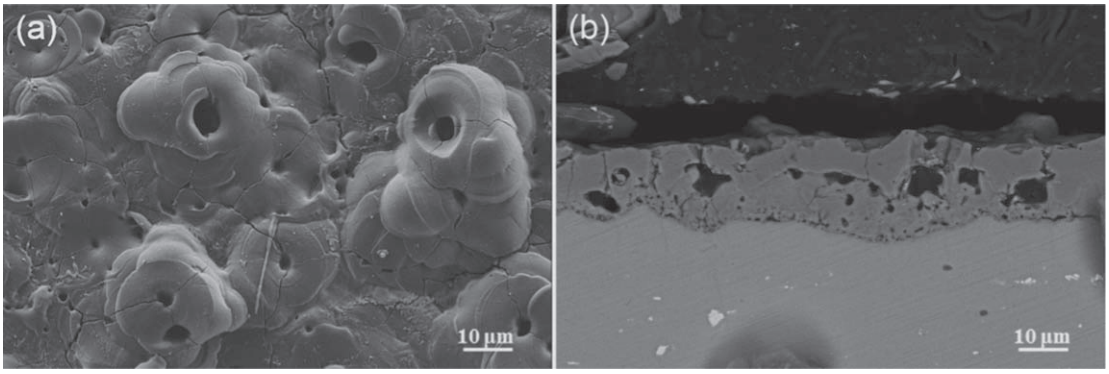

Figure 1. Surface (a) and cross-sectional (b) FESEM micrographs of the MAO coating on 6061 Al alloy.

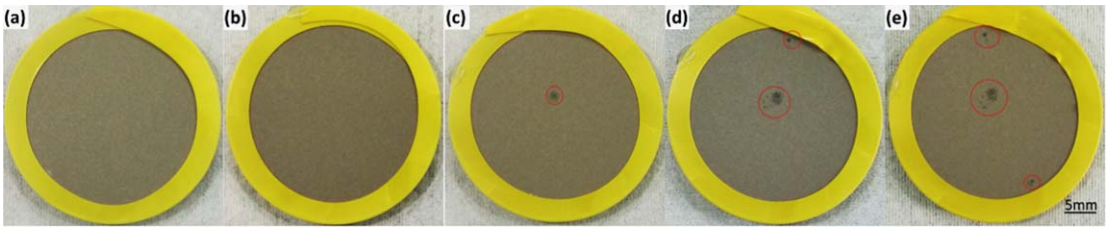

Figure 2. Photographs of the MAO coating on 6061 Al alloy during NSST at different times: (a) 0 h, (b) 480 h, (c) 720 h, (d) 960 h and (e) 1200 h. Corrosion pits are indicated using circles.

universal material testing machine (Jinhua mingke tool equipment Co., Ltd, China) according to standard HB 5476-1991. The tensile rate was 2 mm s^{-1}, and the ultimate tensile strength was determined based on the average of at least three different tensile specimens.

3. Results

3.1. Microstructure of the MAO coating

The surface and cross-section morphologies of the original MAO coating prepared on 6061 Al alloy are shown in figure 1. The surface of the MAO coating was characterized by the typical porous structure along with some micro-cracks. The observed micro-pores are regarded as traces of the plasma discharge, while the micro-cracks result from thermal stresses induced during the MAO process [24, 25]. The surface porosity of MAO/Ag coating was found to be 2.35 $\pm$ 0.16%. In addition, micro-pores and micro-cracks were clearly observed in the cross-section micrograph shown in figure 1(b). They were mostly restricted to the outer layer of the MAO coating, but did not appear to interconnect to the substrate. The MAO coating was integrated firmly with Al substrate by sintered interlocking and the average tensile strength was 60.69 MPa, suggesting a good bonding strength between the coating and the substrate. Outstanding bonding strengths of the MAO coatings have also been reported by other researchers [26, 27]. The average thickness of the MAO coating was determined to be 12.8 μm, as a result of a considerable number of measurements at different positions within the coating.

3.2. Neutral salt spray test (NSST)

Figure 2 presents the surface photographs of the MAO coating during the NSST at different times. After 720 h, obvious pitting corrosion occurred on coating surface, as indicated in figure 2(c) with a red circle surrounding the corrosion pit. As the test time proceeded, corrosion pits widened in size and increased in number, consistent with the sequence of photographs shown in figures 2(d)–(e), corresponding to 960 and 1200 h NSST times, respectively. These NSST results indicated that the MAO coating could protect 6061 Al alloy against the salt spray corrosion for a considerable period of time, taking into account that, without the MAO coating, the corrosion pits would quickly appear after less than 100 h in the uncoated 6061 Al alloy [28].

Detailed corrosion morphologies of the MAO coating after the 1200 h NSST are given in figure 3. It can be seen from figure 3(a) that the slight pitting corrosion was accompanied with the collapse of the surrounding coating and widened micro-cracks. In case of the serious corrosion pit (figure 3(b)), the corrosion area expanded

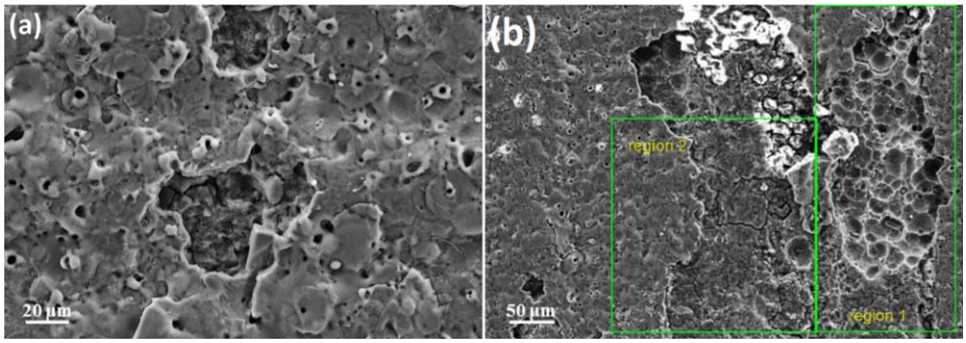

Figure 3. Surface FESEM micrographs of MAO coating after NSST of 1200 h: (a) slight corrosion pit and (b) serious corrosion pit.

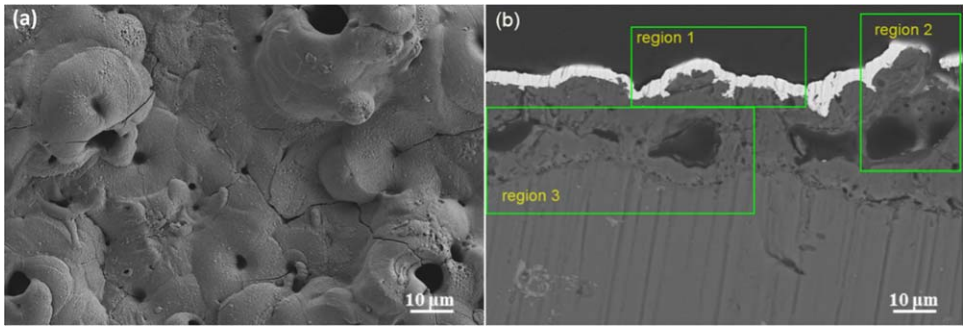

Figure 4. Surface (a) and cross-sectional (b) FESEM micrographs of the MAO-Ag composite coating on 6061 Al alloy.

horizontally in region 1. The salt solution first condensed at the bottom of the holes, where corrosion pit started. As corrosion aggravated, these holes formed an open corrosion pit or an aggregate of such pits with honeycomb-like structure. In contrast, the salt solution penetrated in depth in Region 2, leading to the formation of the widened micro-cracks [29, 30]. In other words, it appears that the solution flowed along the micro-cracks and penetrated gradually into the substrate. The advancement of corrosion thus seems to depend on the protective effect of the inner dense layer of the MAO coating [12, 15].

3.3. Simulation of salt spray corrosion behaviour of MAO coating by laser induced Ag infiltration

Given the microstructure characteristics of the MAO coating, its defects (micro-pores and micro-cracks) were expected to be the channels through which the salt spray penetrated. Besides, pitting corrosion was probably the main cause for the failure of the MAO coating. Thus, in order to corroborate this corrosion scheme, a new laser induced Ag infiltration process was developed and carried out on the original MAO coating after Ag sputtering.

Figure 4 reveals the surface and cross-sectional morphologies of the MAO-Ag composite coating. The outer Ag coating did not apparently change the surface microstructure of the MAO coating, and similar defects, including micro-pores and micro-cracks, could still be found (figure 4(a)). The surface porosity of the MAO/Ag coating (2.35 $\pm$ 0.16%) was similar to that of the MAO coating (2.37 $\pm$ 0.27%). Cross-sectional morphology in figure 4(b) displayed that the MAO coating was covered by a snow-like, white contrast Ag layer with an average thickness of 3.6 μm. The open micro-pores in the near surface were totally filled with Ag particles, as indicated in region 1 of figure 4(b). However, as observed in region 2 of this figure, Ag particles did not fill large cavities, but rather deposited on their walls. Besides, Ag particles were unable to reach the micro-pores in the inner layer of the MAO coating, as observed in region 3 of figure 4(b). Taking into account the above observations, it can be suggested that the defects (micro-pores and micro-cracks) in the near-surface areas of the MAO coating were all in contact with salt spray during the initial stage of the corrosion process. However, there was no indication about where the corrosion channels were located or how they behaved.

The Ag infiltration was initially conducted with a ns n-IR fiber laser. The laser treatment was performed in air using a power of 12 W. The laser beam scanned the surface at 150 mm s^{-1} with a frequency of 1 MHz, displacing each described (scanned) line every 20 μm in the orthogonal direction to the beam scan. The cross-sectional morphology of the MAO/Ag composite coating after laser irradiation is illustrated in figure 5. The infiltrating Ag layers were zone melted by the laser and then solidified into some localized cluster-like aggregates.

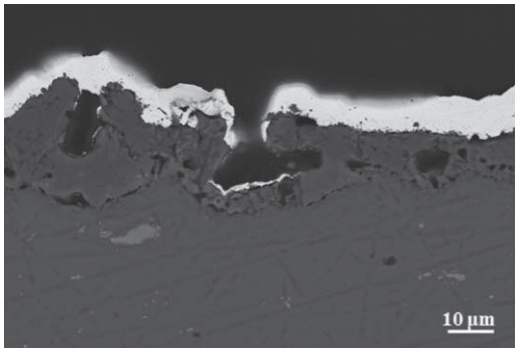

Figure 5. Cross-sectional FESEM micrograph of the MAO/Ag composite coating after the ns n-IR fiber laser irradiation: power 12 W, frequency 1 MHz, laser scanning speed 150 mm s^{-1}, distance between scanning lines 20 μm and single pass.

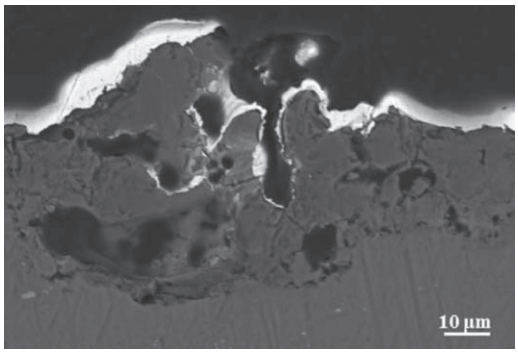

Figure 6. Cross-sectional FESEM micrograph of the MAO/Ag composite coating after the ns n-IR fiber laser irradiation: power 12 W, frequency 1 MHz, laser scanning speed 100 mm s^{-1}, distance between scanning lines 20 μm and single pass.

These Ag aggregates tended to thicken as a response to the thermal effect of near infrared radiation and surface tension effects taking place in the liquid phase during the melting process. Moreover, Ag was detected on the bottom and walls of some blind holes. This indicated that liquid Ag could penetrate into the interior of the MAO coating through microstructure defects, and solidify into a very thin layer of about 1 μm. The salt spray was expected to behave like this Ag liquid, spread into the MAO coating, locally coagulate and converge as corrosive solution on the bottom of blind holes where pitting corrosion started.

Figure 6 gives the cross-sectional morphology of the MAO/Ag composite coating after the ns n-IR fiber laser irradiation at a lower scanning speed 100 mm s^{-1}. When the scanning speed decreased, the energy per unit length deposited on the sample surface enhanced and, consequently, the molten volume of Ag increased. This is accompanied by a decrease in viscosity of the Ag molten pool. Surface tension within the Ag melt became more dominant than its interaction with the pore walls. Thus, Ag was able to diffuse further into the interior of the MAO coating. As time evolved, Ag nanoparticles (similarly the salt spray) should accumulate on the bottom of blind holes and progressively spread into deep holes via micro-cracks, as well as through necking between interlinked holes.

The ps UV laser was used to avoid the agglomeration and condensation of Ag layer on the MAO coating resulting from the surface tension during the melting process. The ps UV laser was able to induce a much lower photothermal contribution, and thus generated a smaller heat affected zones. The laser parameters used in this treatment are the following: nominal pump power 0.75 W, pulse repetition frequency 800 kHz, beam scan speed 5 mm/s, scan length 5 mm, and distance between scaning lines 10 μm for a single beam scan pass. The cross-sectional morphology of the MAO/Ag composite coating and the corresponding Al element distribution after the ps UV laser irradiation are shown in figure 7. The walls of the seemingly isolated holes were covered with Ag nanoparticles, indicating that these holes were essentially interlinked to certain channels which connected the surface of the sample. During NSST, these holes in the MAO coating would be expected to be covered with salt spray.

In order to ensure that the Ag particles penetrated deeply into the interface between the MAO coating and the Al substrate, the MAO/Ag composite coating was irradiated in multi-pass fashion using the UV laser beam at a low scanning speed (2 mm s^{-1}), and the results are shown in figure 8. The prolongation of laser treatment time

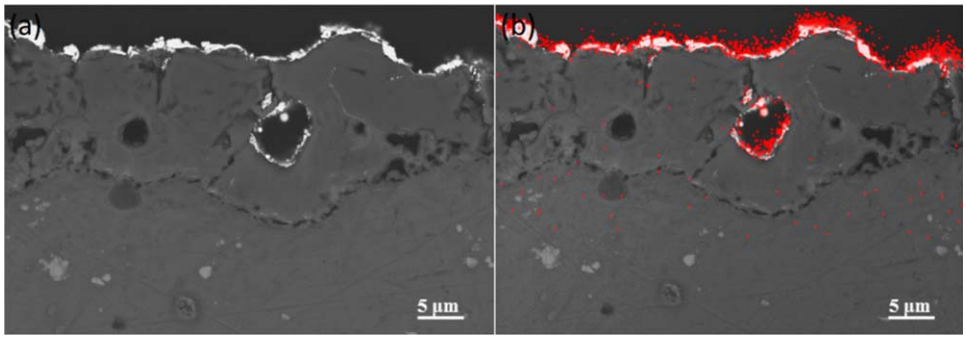

Figure 7. Cross-section FESEM micrograph (a) and corresponding Ag element distribution (b) of the MAO/Ag composite coating after the ps UV laser irradiation: pump power 0.75 W, frequency 800 KHz, scanning speed 5 mm/s, distance between scanning lines 10 μm and single pass.

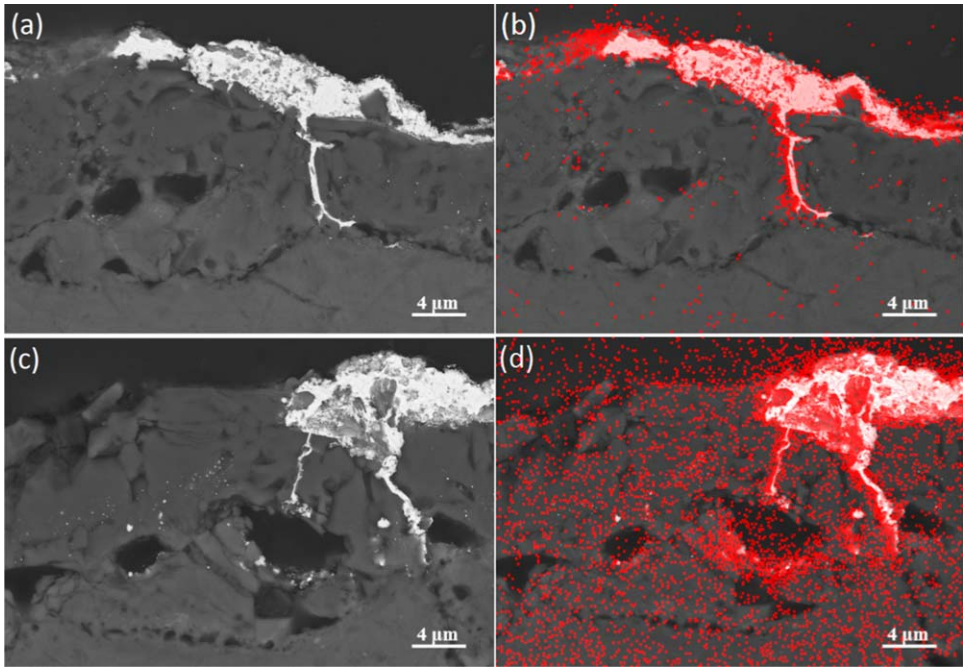

Figure 8. Cross-section FESEM micrograph (a), (c) and corresponding Ag element distribution (b), (d) of the MAO-Ag composite coating after the ps UV laser irradiation: pump power 1.4 W, frequency 800 KHz, scanning speed 2 mm s^{-1}, distance between scanning lines 50 μm, defocusing amount 2 mm and 12 passes with start angle increasing 30° per pass.

promoted further diffusion of Ag along the micro-cracks network generated during the MAO process, and into the holes located near the MAO coating/substrate interface. These results provided the direct experimental evidence to support the idea that some micro-cracks in MAO coatings appear in the shape of tree root or lightning. During the NSST, these micro-cracks would therefore account for the presence of at least one type of corrosion channel.

4. Discussion

The NSST is a commonly used method to evaluate the corrosion resistance of the MAO coating on Al alloys. However, it was difficult to trace the corrosion sequential process and observe corrosion channels induced during the NSST. This is mainly because most corrosion channels were locally destroyed due to the formation of corrosion products during the NSST. Moreover, the distribution of corrosion products inside the MAO coating could be damaged during sample preparation (including sample cutting and polishing). This work explores a laser induced Ag infiltration process in order to ascertain possible ways to simulate the corrosion behaviour of the MAO coating during the NSST. The penetration of salt spray into the MAO coating behaved like the infiltration of Ag particles induced by laser treatment of a Ag sputtered MAO coated alloy. The new laser induced

Ag infiltration process presented here, to our knowledge, has not been previously reported in the scientific literature. Under appropriate ps UV laser irradiation conditions, in the Laser beam scan mode of operation, the sputtered Ag layer was able to reach the proximities of the interface between the MAO coating and Al alloy substrate. The results of the laser induced Ag infiltration presented above, indicated that the potential corrosion channels of the MAO coating mainly consisted of micro-pores, large cavities far beneath the surface and tree-root like micro-cracks. Through these corrosion channels, the salt spray was capable of spreading deeply into the whole MAO coating in the cross-sectional direction and towards the MAO coating/alloy substrate interface.

Based on the results of the laser induced Ag infiltration, during the NSST, the micro-pores and micro-cracks within the surface area of the MAO coating were all in intimate contact with the salt spray at the beginning stage of the test. The salt spray may accumulate at the bottom of the observed blind holes and progressively spread into deeper holes via micro-cracks, as well as via the observed network between interlinked holes (figures 5–7). The chloride ion (Cl^-) has strong adsorption capacity and erosiveness, which is the principal cause of pitting corrosion [31]. The salt solution condensed at the bottom of the hole, where corrosion pit started. As the corrosion process evolved, these holes formed an open corrosion pit or an aggregate of such pits with honeycomb-like structure. Meanwhile, the original micro-cracks became widened, which was more conducive to the penetration of the salt solution [29, 30]. The corrosion progress largely depended on the protective effect of the dense inner layer of the MAO coating [15]. When salt spray arrived at the interface between MAO coating and substrate, the latter began to suffer corrosion because of its high chemical activity. In addition, however, the presence of micro-cracks reaching the MAO coating/substrate interface has been observed (figure 8). These are proposed to accelerate the corrosion process of the Al alloy substrate. The accumulation and blockage of corrosion products within these micro-cracks could delay the penetration process of the salt spray during the NSST, and is proposed as a measure to delay corrosion kinetics of the MAO protected alloy.

In view of the above, the results of this work are of significant importance towards understanding the behaviour of the MAO coatings under various corrosive environments before pitting. In addition, the laser induced Ag infiltration process directly proves the presence of some micro-cracks with tree root or lightning shape within the MAO coating (figure 8), which may also suggest ways to better understand the discharge mechanism inherent to the MAO process.

5. Conclusions

A new laser induced melting method was applied over the sputtered Ag layers previously deposited on the MAO coated Al alloy. Irradiation under laser beam scan (LBS) mode yielded a controlled, molten Ag layer. This molten Ag layer was able to penetrate through the typical micro-pore and micro-crack structure intrinsic to MAO coatings, thus opening the way to comprehend how such a structure may play a role in the corrosion mechanism of the MAO coated Al alloy. The use of nIR or UV lasers with different pulse regimes enabled controlling the Ag molten layer as well as the thermal input which, in turn, allowed controlling Ag melt penetration. In this manner, Ag penetration via small micro-pores and micro-cracks was assured, as demonstrated with electron microscopy studies. These may help, through further studies, to increase the understanding of these MAO coating structures, and thus design improved protective, anticorrosion coatings. Moreover, the results of Ag infiltration under laser irradiation directly proved the presence of tree root or lightning shaped micro-cracks within the MAO coating.

Acknowledgments

This research was funded by National Natural Science Foundation of China (No. 51901099) and China Postdoctoral Science Foundation (No. 51203237). Partial funding from Gobierno de Aragón 'Construyendo Europa desde Aragón' (research group T54_17R) is acknowledged, along with the use of Servicio General de Apoyo a la Investigación-SAI, Universidad de Zaragoza.

ORCID iDs

Cancan Liu https://orcid.org/0000-0002-3601-2500
Hongtao Li https://orcid.org/0000-0002-0416-4737
L A Angurel https://orcid.org/0000-0001-5685-2366
Bailing Jiang https://orcid.org/0000-0003-3547-4460

References

[1] Curran J A, Kalkancı H, Magurova Y and Clyne T W 2007 *Surf. Coat. Technol.* **201** 8683
[2] Kim D, Sung D, Lee J, Kim Y and Chung W 2015 *Appl. Surf. Sci.* **357** 1396
[3] Huang Q *et al* 2019 *Surf. Coat. Technol.* **374** 1015
[4] Yerokhin A L, Nie X, Leyland A and Matthews A 2000 *Surf. Coat. Technol.* **130** 195
[5] Xue W B, Deng Z W, Lai Y C and Chen R Y 1998 *J. Am. Ceram. Soc.* **81** 1365
[6] Gnedenkov S V, Gordienko P S, Khrisanfova O A, Scorobogatova T M and Sinebrukhov S L 2002 *J. Mater. Sci.* **37** 2263
[7] Shamsi F, Khorasanian M and Lari Baghal S M 2018 *Surf. Coat. Technol.* **346** 63
[8] Shishavan B H, Khosrowshahi R A, Shishavan S H, Samani M N and Ahmadi N P 2019 *Appl. Surf. Sci.* **481** 108
[9] Fatimah S, Kamil M P, Kwon J H, Kaseem M and Ko Y G 2017 *J. Alloys Compd.* **707** 358
[10] Sun S Q, Wu G Q, Sun L B, Shan X P, Li M Y and Ji S D 2018 *Mater. Res. Express* **5** 116506
[11] Liu Y F, Liskiewicz T, Yerokhin A, Korenyi-Both A, Zabinski J, Lin M Y, Matthews A and Voevodin A A 2018 *Surf. Coat. Technol.* **352** 238
[12] Liu C, Liu P, Huang Z Q, Yan Q, Guo R G, Li D L, Jiang G R and Shen D J 2016 *Surf. Coat. Technol.* **286** 223
[13] Deng H C, Ma Z Z, Zhang X L, Zhang Y F and Liu X W 2015 *Surf. Coat. Technol.* **269** 108
[14] Kong D J and Wang J C 2015 *J. Alloys Compd.* **632** 286
[15] Shao L L, Li H T, Jiang B L, Liu C C, Gu X and Chen D C 2018 *Metals* **8** 165
[16] Wang Y, Huang Z Q, Yan Q, Liu C, Liu P, Zhang Y, Guo C H, Jiang G R and Shen D J 2016 *Appl. Surf. Sci.* **378** 435
[17] Jiu J T, Nogi M, Sugahara T, Tokuno T, Araki T, Komoda N, Suganuma K, Uchida H and Shinozaki K 2012 *J. Mater. Chem.* **22** 23561
[18] Hu L B, Kim H S, Lee J Y, Peumans P and Cui Y 2010 *ACS Nano* **4** 2955
[19] Li H X, Rudnev V S, Zheng X H, Yarovaya T P and Song R G 2008 *J. Alloys Compd.* **462** 99
[20] Martin J, Nominé A, Ntomprougkidis V, Migot S, Bruyère S, Soldera F, Belmonte T and Henrion G 2019 *Mater. Design* **180** 107977
[21] Olakanmi E O, Cochrane R F and Dalgarno K W 2015 *Prog. Mater. Sci.* **74** 401
[22] Sánchez-Valencia J R, Toudert J, Borras A, Barranco A, Lahoz R, de la Fuente G F, Frutos F and Gonzalez-Elipe A R 2011 *Adv. Mater.* **23** 848
[23] Rico V R, López-Santos C, Villagra M, Espinos J P, de la Fuente G F, Angurel L A, Borras A and Gonzalez-Elipe A R 2019 *Langmuir* **35** 6483
[24] Fadaee H and Javidi M 2014 *J. Alloys Compd.* **604** 36
[25] Kaseem M, Kamil M P, Kwon J H and Ko Y G 2015 *Surf. Coat. Technol.* **283** 268
[26] Li K, Li W F, Zhang G G, Zhu W, Zheng F H, Zhang D Q and Wang M 2019 *J. Alloys Compd.* **790** 650
[27] Tran Q P, Sun J K, Kuo Y C, Tseng C Y, He J L and Chin T S 2017 *J. Alloys Compd.* **697** 326
[28] Leggat R B, Taylor S R, Zhang W and Buchheit R G 2002 *Corros.* **58** 283
[29] Barati N, Yerokhin A, Golestanifard F, Rastegari S and Meletis E I 2017 *J. Alloys Compd.* **724** 435
[30] Wen L, Wang Y, Zhou Y, Ouyang J H, Guo L and Jia D 2010 *Corros. Sci.* **52** 2687
[31] Santana R J J, Javier S H F and Gonzalez J E 2003 *Corros. Sci.* **45** 799